Supporting Information

Creating Edge Sites within the Basal Plane of MoS$_2$ Catalyst for Substantially Enhanced Hydrodeoxygenation Activity

Kui Wu, [†] Xinxin Li, [‡] Weiyan Wang, *, [†] Yanping Huang, [†] Qike Jiang, [§] Wensong Li, [†] Yuanqiu Chen, [†] Yunquan Yang [†] and Changzhi Li* [‡]

[†] School of Chemical Engineering, Xiangtan University, Xiangtan, Hunan, 411105, P.R. China

[‡] CAS Key Laboratory of Science and Technology on Applied Catalysis, Dalian Institute of Chemical Physics, Chinese Academy of Sciences, Dalian 116023, P. R. China

[§] Dalian National Laboratory for Clean Energy, Dalian Institute of Chemical Physics, Chinese Academy of Sciences, 457 Zhongshan Road Dalian 116023, China

* To whom correspondence should be addressed.

E−mail: wangweiyan@xtu.edu.cn (W. Wang), licz@dicp.ac.cn (C. Li)

Experimental Methods

1. Catalyst characterizations

X−ray diffraction (XRD) measurements were carried on a D/max 2500 18KW Rotating anode X−Ray Diffractometer with monochromatic Cu Kα radiation (λ＝1.5418 Å) radiation at the voltage and current of 40 kV and 250 mA, respectively. Field emission scanning electron microscope (FE−SEM) images were recorded on a JSM−6700F scanning electron microscope. The 2θ was scanned over the range of 5−90 ° at a rate of 10 °/min. The specific surface area was measured by a Quantachrome's NOVA−2100e Surface Area instrument by physisorption of nitrogen at 77 K. The samples were dehydrated at 300 °C using vacuum degassing for 12 h before experiments. The morphologies of catalysts were determined by high−resolution transmission electron microscopy (HRTEM) on a JEOL JEM−2100 transmission electron microscope with a lattice resolution of 0.19 nm and an accelerating voltage of 200 kV. The samples for the TEM study were prepared by the ultrasonic dispersing in ethanol and consequent deposition of the suspension upon a lacey support film. Extended X−ray absorption fine structure (EXAFS) analyses of the Co K−edge was carried out on the BL14W1 beamline of the Shanghai Synchrotron Radiation Facility (SSRF) at 3.5 GeV with a maximum current of 200 mA. The acquired EXAFS data were processed according to the standard procedures using the ATHENA module implemented in the IFEFFIT software packages. The atomic resolution microscopy analysis was performed on a JEM ARM200F thermal−field emission microscope with a probe spherical aberration (Cs) corrector working at 80 kV. X−ray photoelectron spectroscopy (XPS) was recorded on a Thermo Scientific K−Alpha X−ray photoelectron spectrometer. All XPS spectra were corrected to the C 1s peak at 284.6 eV. The DE convolution of the XPS signal was performed on avantage software. The samples were also inspected by using Raman spectroscopy using a Renishaw inVia confocal Raman microscope with

a 532 nm excitation Laser. For fixing and levelling the powder, a PXRD quartz sample stage with groove was employed as microslide. The metal contents in the solids were analysed by plasma coupled atomic emission spectroscopy (ICP−AES).

2. Activity test

2.1 Hydrodeoxygenation of model compounds on Pt−MoS$_{2-x}$

The prepared catalyst without any further treatment (0.1 g), p−cresol (2.4 g) and dodecane (15.0 g) was placed into a 100−mL sealed autoclave. Air in the autoclave was evacuated by pressurization−depressurization cycles with nitrogen and subsequently with hydrogen. After the system temperature reached the set point, the autoclave was then pressurized with hydrogen and the stirring speed was adjusted to 900 rpm. During the reaction, liquid samples were withdrawn from the reactor and analysed by Agilent 6890/5973N GC−MS and 7890 gas chromatography using a flame ionization detector (FID) with a 30 m AT−5 capillary column. To separate the reaction products, the temperature in the GC oven was increased from 40 °C to 85 °C with the ramp rate of 20 °C/min, held at 85 °C for 4.0 min, then increased to 200 °C at a ramp rate of 20 °C/min and finally kept at 200 °C for 5.0 min. The HDO experiments (except for catalytic stability test) were repeated at least twice at a single condition and the results showed that the standard deviations of conversion and selectivity were less than 3.0%. The conversion, selectivity and deoxygenation degree for each experiment were calculated as follows:

$$\text{Conversion (mol \%)} = \left(1 - \frac{\text{moles of residual } p - \text{cresol}}{\text{moles of initial } p - \text{cresol}}\right) \times 100\%$$

$$\text{Selectivity (A, mol\%)} = \frac{\text{moles of product (A)}}{\text{moles of reacted } p - \text{cresol}} \times 100\%$$

Deoxygenation degree (D.D., wt%)

$$= \left(1 - \frac{oxygen\ content\ in\ the\ final\ organic\ compounds}{total\ oxygen\ content\ in\ the\ initial\ mixture}\right) \times 100\%$$

2.2 Catalyst recycling test

After reaction, the spent catalyst was separated from the reaction system by centrifugation, washed with a large quantity of ethanol, and dried at 80 °C for 4 h under vacuum. After that, the recycled catalyst was reused directly for the next run.

2.3 Hydrodeoxygenation of lignin oil on Pt−MoS$_{2−x}$

Lignin oil (100 mg), Pt−MoS$_{2−x}$ catalyst (100 mg), and n−hexane (15 mL) were added to a 50 mL autoclave. The reaction was performed at 260 °C with 4 MPa H$_2$ and 20 h for the conversion of lignin oil. After the reaction, the reaction mixture was cooled rapidly to room temperature and filtered. The filtrate was analyzed by using GC−MS and quantified by GC−FID using an internal standard (standard: n−tridecane, HP−5 column, 30 m × 0.32 mm × 0.25 □m). The filtrate was concentrated at RT overnight to obtain liquid oil. The monomers (i.e. cyclohexane, methylcyclohexane, ethylcyclohexane, butylcyclopentane, propylcyclohexane) were evaporated with the solvent in the concentration process because of their low boiling points, thus did not exist in the oily hydrocarbons.

3. Density functional theory calculations

The density functional theory (DFT) calculations were performed with the Vienna ab initio simulation package (VASP) code. The projector augmented wave (PAW) method was applied to describe the interaction between electrons and the ionic cores. Electron exchange−correlation was represented by the functional of Perdew−Burke−Ernzerhof (PBE) of general gradient approximation (GGA). The cutoff of the energy for plane−wave basis was set to 500 eV. To avoid

the interaction between the neighboring periodic structures, all periodic slab calculations were carried out using a vacuum spacing of at least 15 Å. The convergence tolerance was 2×10^{-5} eV and 0.02 eV/Å for energy and force, respectively. And the transition states searching were obtained by relaxing the force below 0.05 eV/Å. The Brillouin−zone integrations were performed by using 3×3×1 Monkhorst−Pack for geometric optimization and energy calculation. In addition, DFT−D3 calculations were used to describe the van der Waals (vdW) interaction. The climbing−image nudged elastic band (CI−NEB) method was applied to determine the minimum energy pathways.
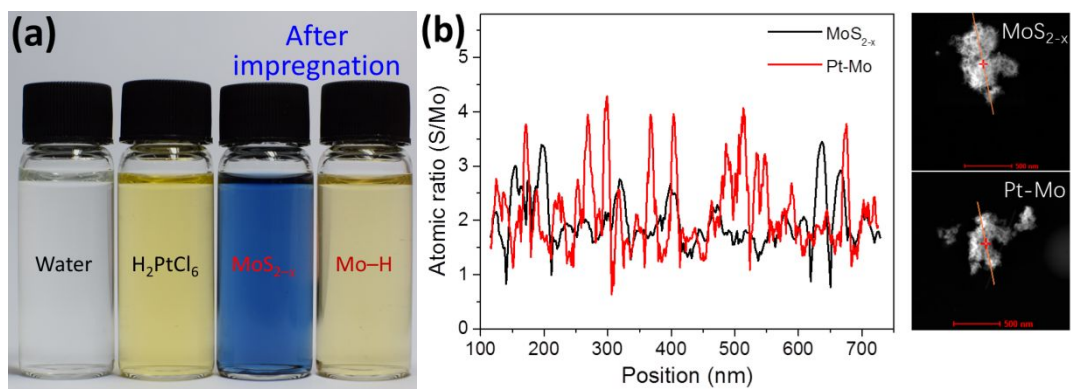
Figure S1. (a) The photo of filtered solution before and after impregnation and (b) S/Mo atom

ratio in MoS_{2-x} and Pt−Mo
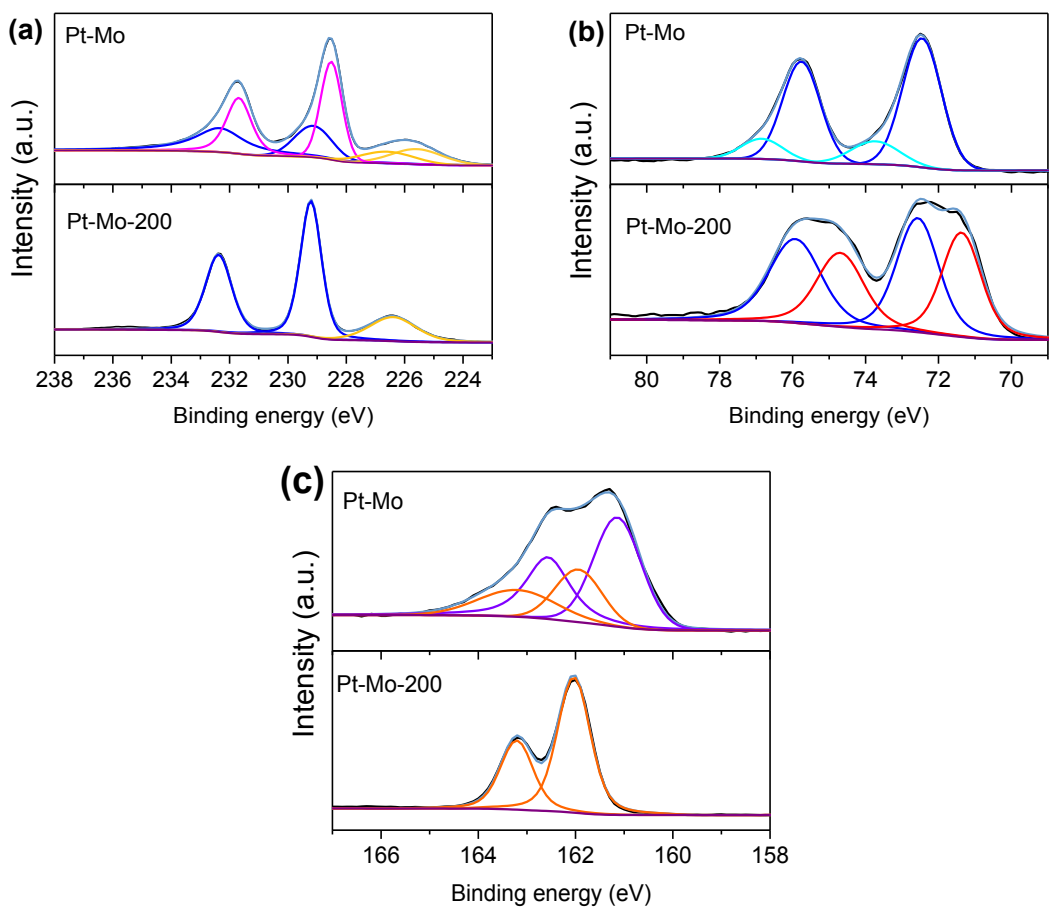
Figure S2. High resolution XPS spectras of (a) Mo 3d, (b) Pt 2p and (c) S 2p regions for of

Pt−MoS_{2-x} catalysts
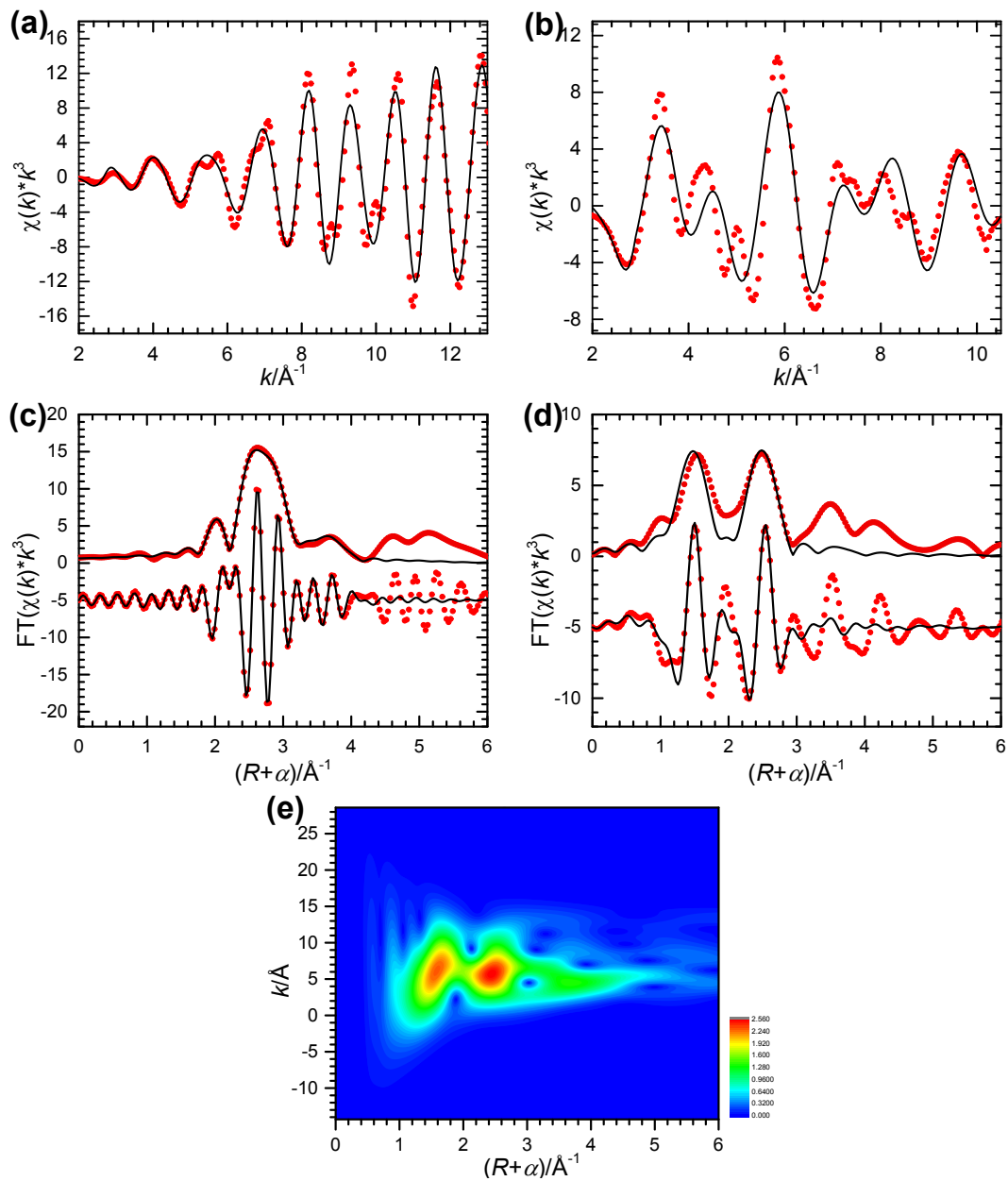
Figure S3. Pt L3-edge EXAFS (point) and the curvefit (line) for (a) Pt foil and (b) Pt-Mo-200 shown in *k*-space; Pt L3-edge EXAFS (point) and the curvefit (line) for (c) Pt foil and (d) Pt-Mo-200 shown in *R*-space (FT magnitude and imaginary component); (e) Wavelet-Transform curves of Pt L3-edge of Pt-Mo-200 shown in *R*-space. The data were k^3 weighted and not phase-corrected.

EXAFS spectra of Pt-Mo-200 was refined by the *Athena* software (*version 0.9.26)*, as shown in Figure S3. The ghost peak at about 1.1 Å was weaken by reducing the Rkbg value to the half distance of the first intensity maximum at about 1.6 Å in *R*-space, and the noise of curve was modified by deglitching and optimizing the selected k range and. After fitting analysis of Pt L3-edge of Pt foil at the range of $1.0 \leq R \leq 4.0$ Å in *R*-space (Figure S3a and S3c), the returned *R*-factor was 0.0050, being lower than the acknowledged fitting error factor (0.02), which indicated that this fitting operation was valid and reasonable. The outputted bond distance of Pt-Pt1 (first shell) and Pt-Pt2 (second shell) was 2.77 and 3.91 Å, respectively, which were consistent with the results in previous literature (*Angew Chem Int Ed*, 2019, 58, 16038). Consequently, we fixed the amplitude reduction factor (S_0) according to the EXAFS fitting of Pt foil and then fitted the Pt L3-edge of Pt-Mo-200 at the *R*-space range of $1.0 \leq R \leq 3.0$ Å, as shown in Figure S3b and S3d. The returned coordination number for Pt-Pt was 4.7, which indicated the small atom cluster of metallic Pt and illustrated the local structure of Pt in Pt-Mo-200 catalyst. The outputted bond distances for Pt-O and Pt-Pt were 1.92 and 2.73 Å, respectively. The Pt-O bond distance was slightly longer than that in PtO_2 (*Nat Mater*, 2019, 18, 746), which may be due to the reacted O atom on Pt surface. However, the Pt-Pt bond distance was shorter than that in Pt foil, which was resulted from the contraction effect of small Pt atom cluster (*Phys Rev Lett*, 1979, 43, 2). Unfortunately, the *R*-factor in this fitting analysis was 0.0332, which was slightly higher than the acknowledged fitting error factor (0.02) even though lots of fittings had been tried to carry out. This was mainly caused by the irregularity of Pt species, the interaction between Pt and MoS_{2-x}, uncertain coordination, measurement indeterminacy, and so on. Furthermore, EXAFS wavelet transform (WT) analysis of Pt-Mo-200 was performed. As shown in Figure S3e, two intensity maximums at about 1.6 and 2.6 $Å^{-1}$ (no phase correction) were observed in the WT contour plot of Pt-Mo-200, indexing to the

coordination contribution between Pt core and other atoms, which was in accordance with the results in k^3 weighted *R*-space. The detailed fitting values (coordination number, bond distance, delta E0, Debye Waller factor, Residual factors) were listed in Table S1.
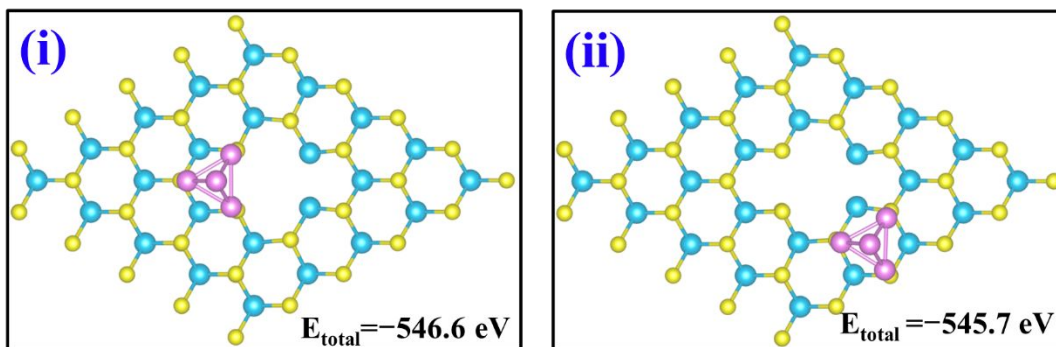
Figure S4. Two configurations of Pt cluster locating on MoS$_{2-x}$

Two Pt cluster location models were built: at edge sites (i) and without at edge sites (ii), as shown in Figure S4. The calculation result indicated that the value of the total energy for configuration (i) was lowered about 0.9 eV in comparison with configuration (ii), suggesting that the configuration (i) was more stable, which was well consistent with the HAADF−STEM result. These demonstrated that the reduced Pt clusters were located at edge sites of MoS$_2$ and then form metal−edge interface. Consequently, configuration (i) was selected to further analyse the adsorption energies of reactant the energy barriers of the reaction steps in the HDO of p−cresol on Pt/MoS$_{2-x}$.
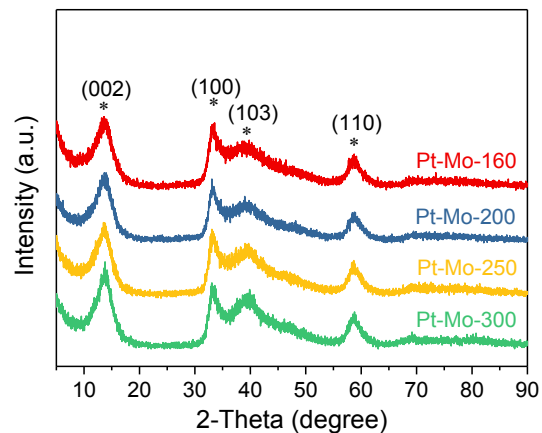
Figure S5. XRD patterns of Pt–MoS$_{2-x}$ heat−treated under different temperatures
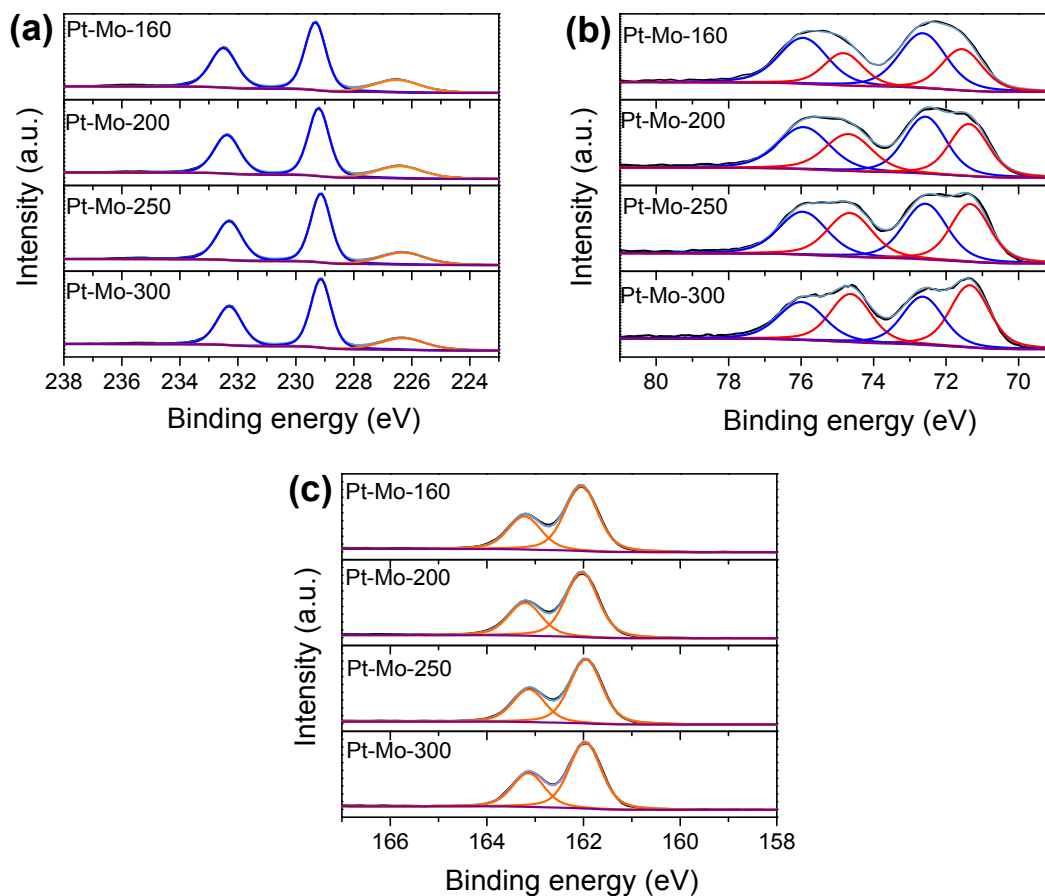
Figure S6. XPS spectra of (a) Mo 3d, (b) Pt 2p and (c) S 2p regions for Pt−MoS$_{2-x}$ pretreated in hydrogen atmosphere at different temperatures
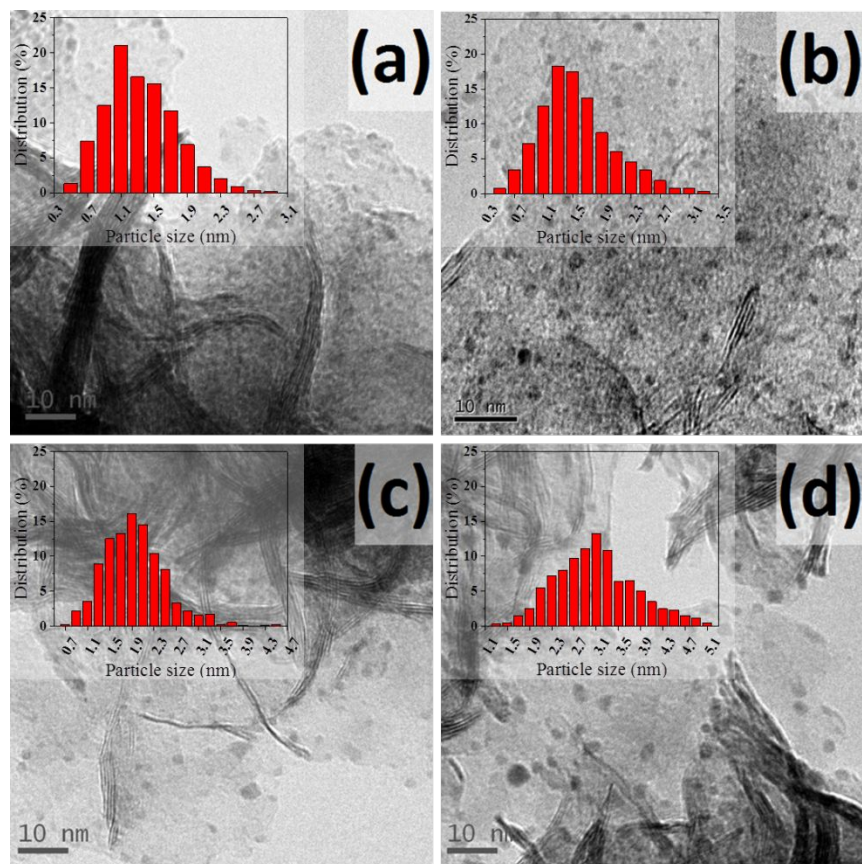
Figure S7. TEM images and particle size distribution of (a) Pt–Mo–160, (b) Pt–Mo–200, (c) Pt–Mo–250 and (d) Pt–Mo–300 catalysts
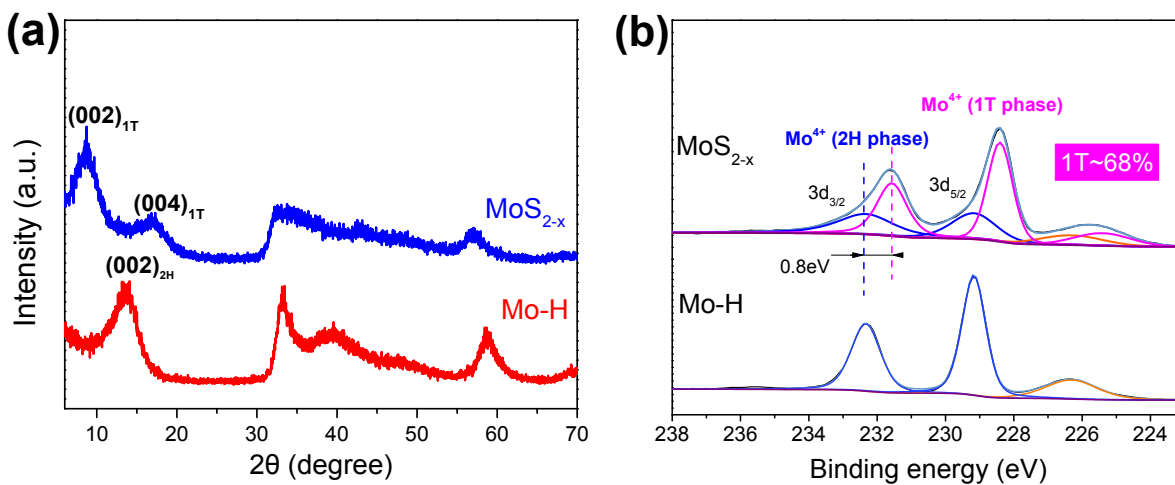
Figure S8. (a) XRD pattern and (b) XPS spectra of Mo 3d region of the as–synthesized and heat–treatment MoS_{2-x} catalysts.
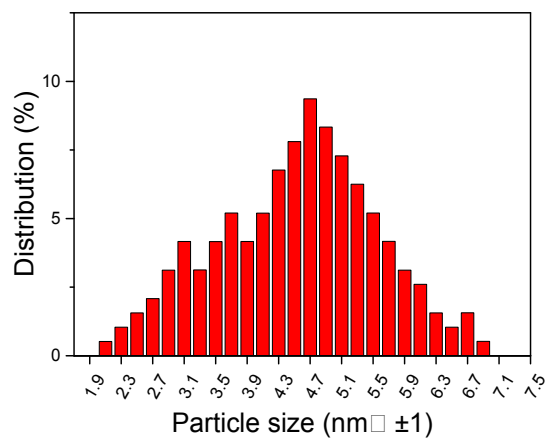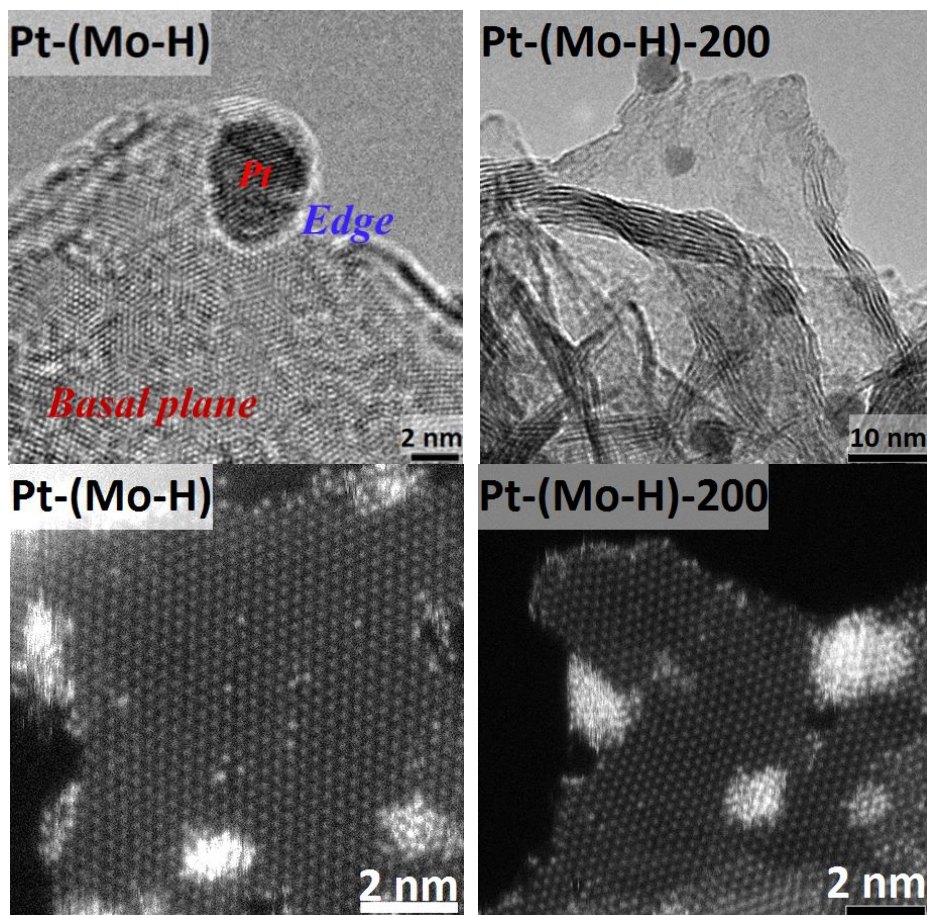
Figure S9. HRTEM and HAADF−STEM images of Pt−(Mo−H) and Pt−(Mo−H)−200 and

particle size distribution of Pt in Pt−(Mo−H)−200
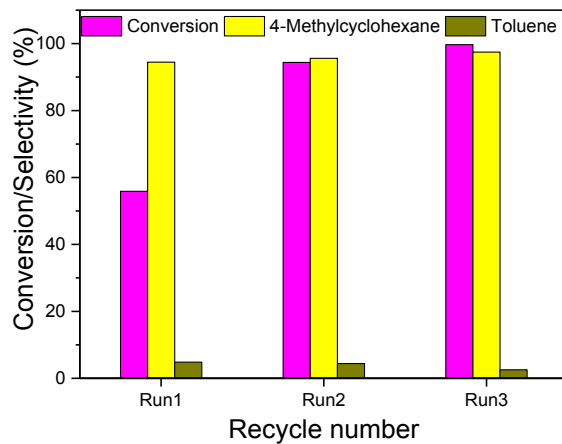
Figure S10. Stability test of Pt−Mo for HDO of *p*−cresol. Reaction conditions: 2.4 g *p*−cresol, 0.1 g catalyst, 5 MPa hydrogen pressure, temperature 160 °C and time 2 h.
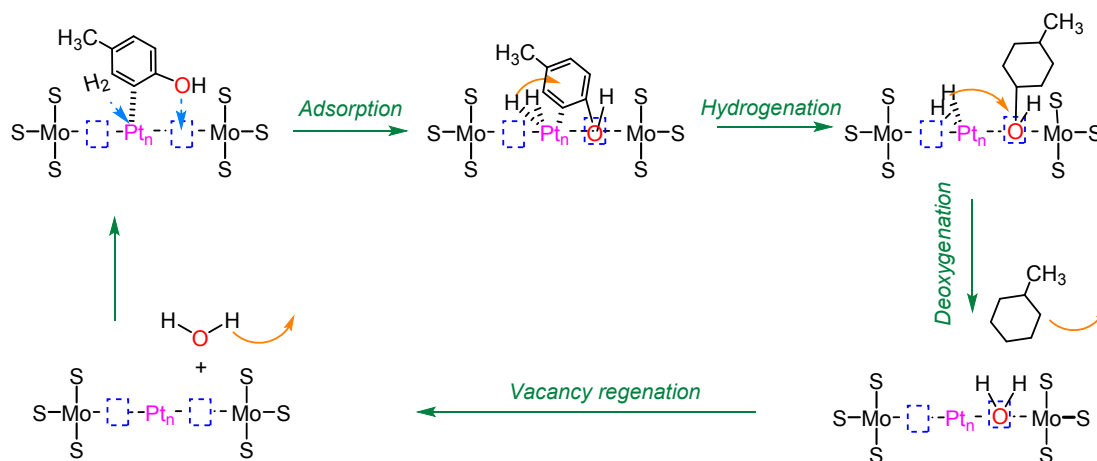
Figure S11. The reaction mechanism for in HDO of *p*−cresol on Pt−MoS$_{2-x}$ catalyst
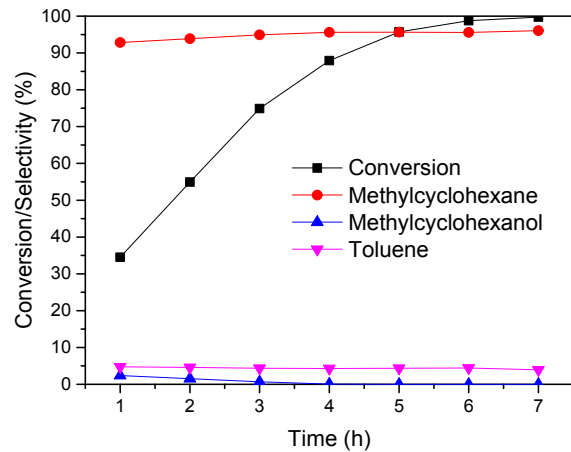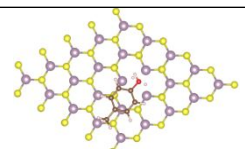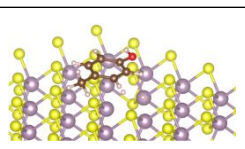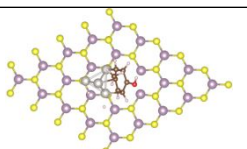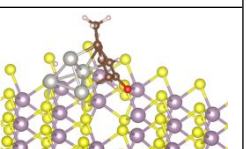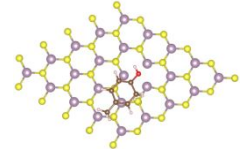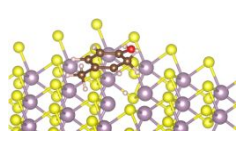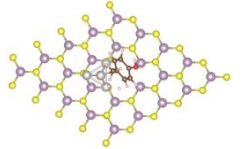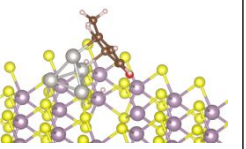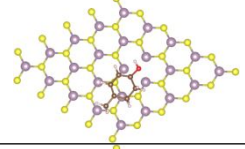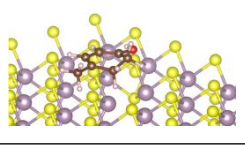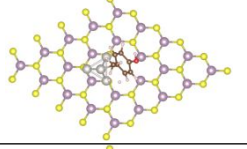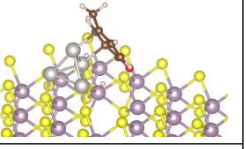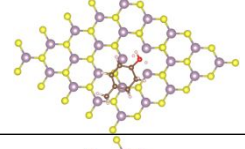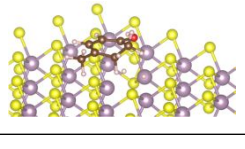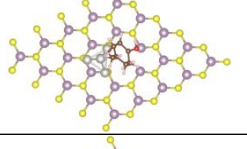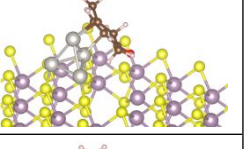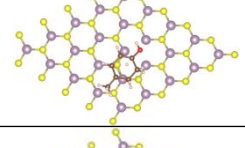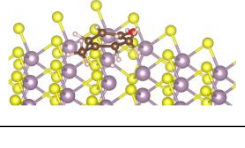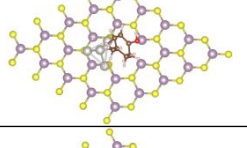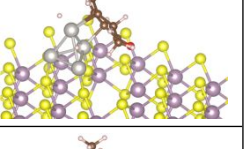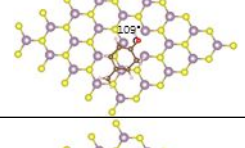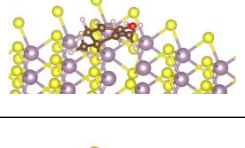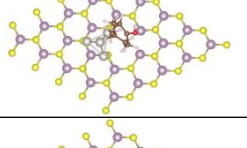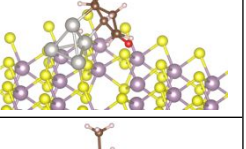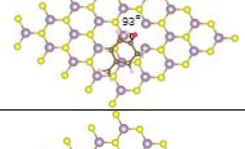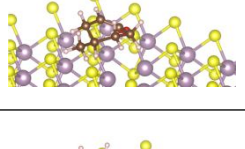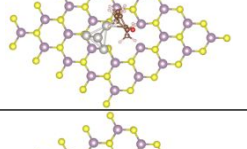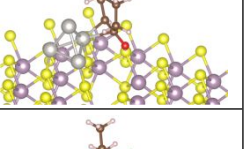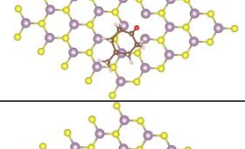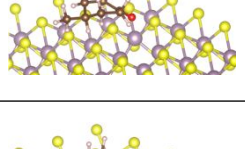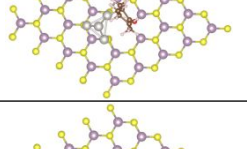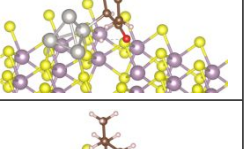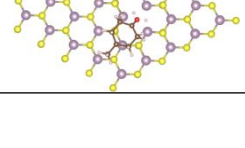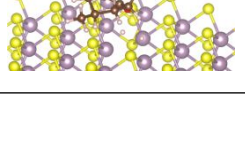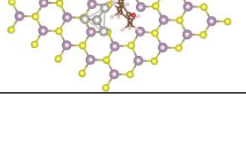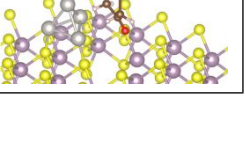
Figure S12. The changes of conversion and product selectivity versus reaction time in HDO of

p−cresol on Pt–Mo–160 at 140 ºC

No.	MoS$_{2-x}$		Pt−MoS$_{2-x}$	
	Top view	Local side view	Top view	Local side view
IS1				
TS1				
FS1				
IS2				
TS2				
FS2 &IS3				
TS3				
FS3				
IS4				

TS4				
FS4 &IS5				
TS5				
FS5				
IS6				
TS6				
FS6 &IS7				
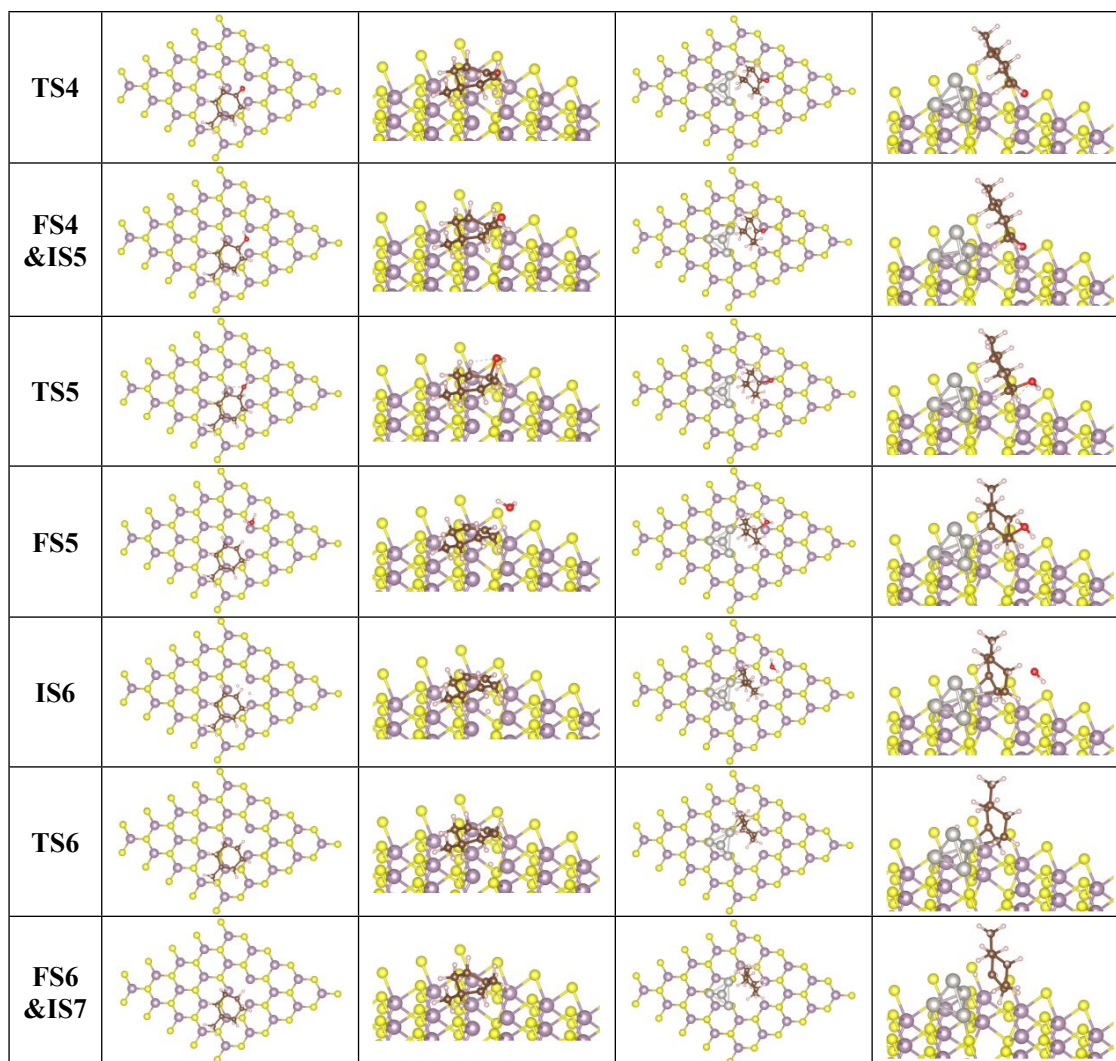
Figure S13. Top and local side views of DFT−optimized structure for initial state (IS), transition state (TS), and final state (FS) of p−cresol HDO via HYD path on MoS_{2-x}, and Pt−MoS_{2-x}

Figure S14. XRD patterns (a) and XPS spectra of (b) Pt 2p, (c) Mo 3d, and (d) S 2p regions for

fresh and spent Pt–Mo–200

Figure S15. GC−MS/FID analysis of the lignin−derived bio−oil
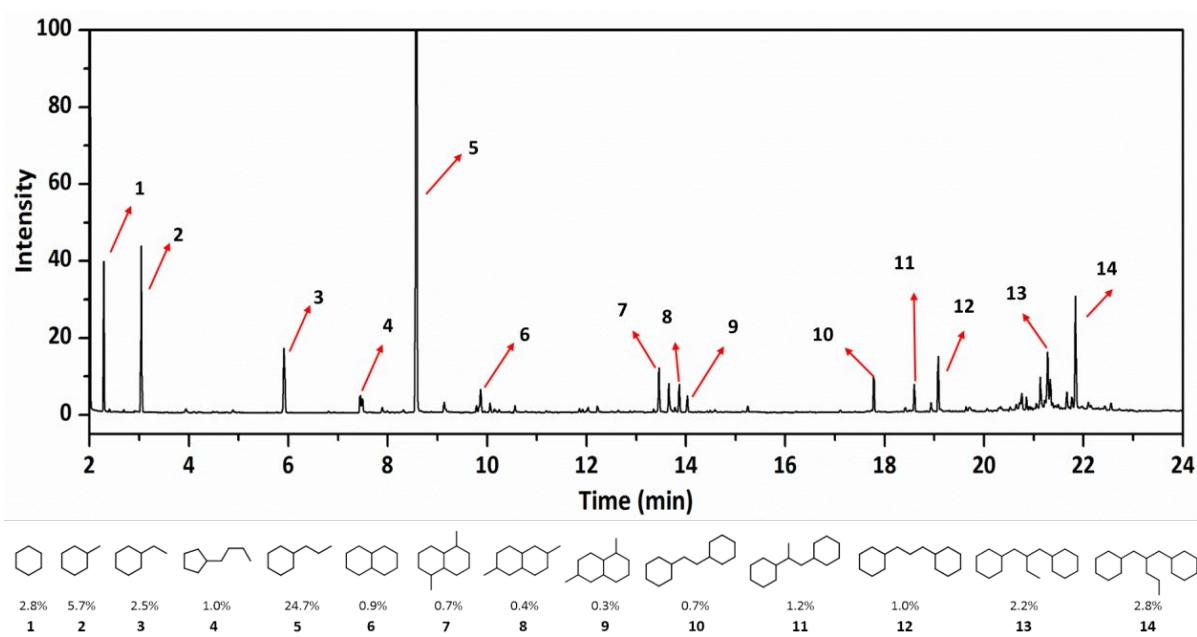
Figure S16. GC−MS/FID analysis of the upgraded lignin bio−oil

Table S1. EXAFS fitting parameters at the Pt L3-edge for Pt foil and Pt-Mo-200[a]

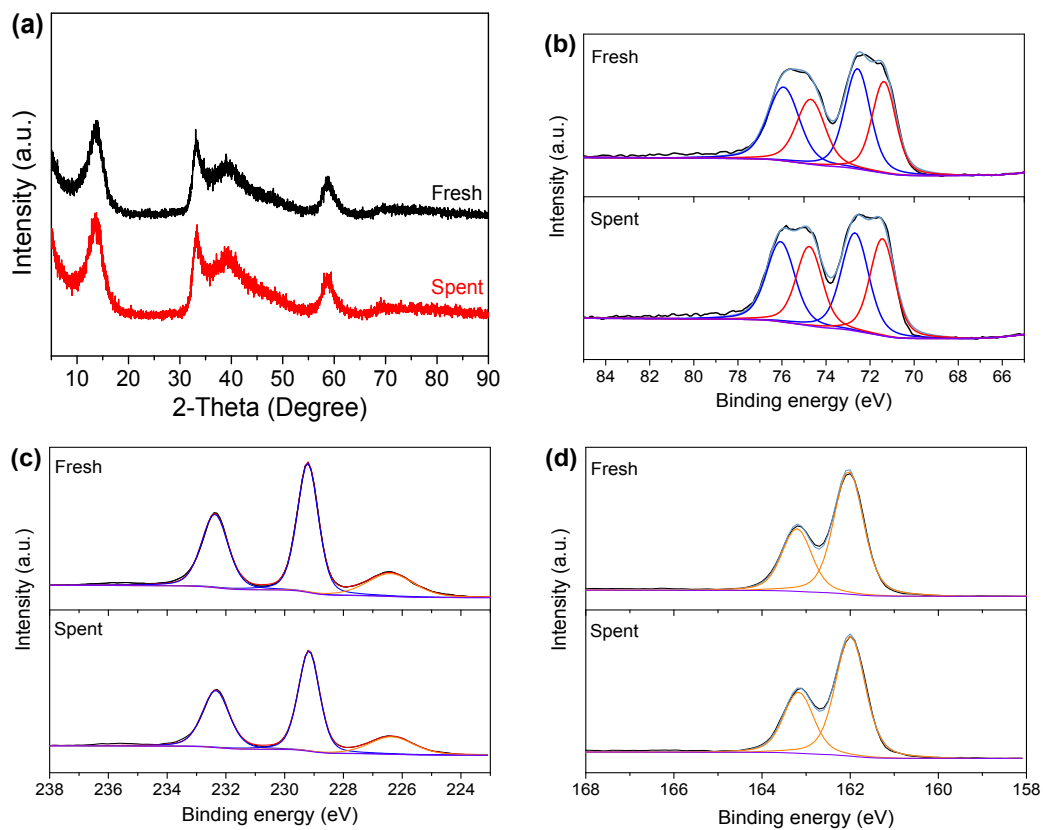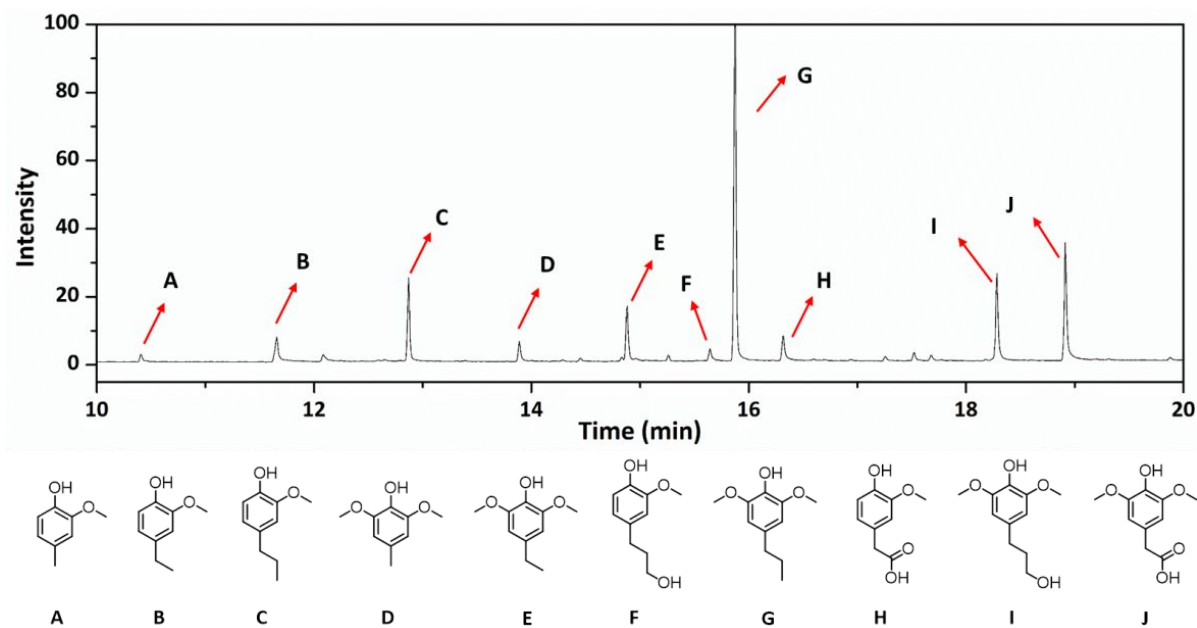| Sample	Path	N[b]	R (Å)[c]	$\triangle E_0$ (eV)[d]	σ^2 (Å²)[e]	R factor[f]
Pt foil	Pt-Pt1	10.7	2.77	8.70	0.0042	0.0050
	Pt-Pt2	3.6	3.91		0.0051	
Pt-Mo-200	Pt-O	0.9	1.82	6.43	0.006	0.0332
	Pt-Pt	4.7	2.73		0.018	

[a] S^0 was fixed as 0.95, according to the experimental EXAFS fit of Pt foil. $\triangle E_0$ was a refined as a global fit parameter for the same sample. Data ranges: $3.0 \leq k \leq 12.5$ and $1.0 \leq R \leq 4.0$ Å for Pt foil; $2.0 \leq k \leq 10.0$ and $1.0 \leq R \leq 3.0$ Å for Pt foil. [b]N: coordination numbers; [c]R: bond distance , the value is obtained by subtracting $\triangle R$ from the path based on the crystal structure. [d] $\triangle E_0$: the inner potential correction; [e]σ^2: Debye-Waller factor; [f]R factor: goodness of fitting.

Table S2. Ion concentration in the remaining solution after impregnation measured by using

atomic absorption spectroscopy

Catalyst	Substrate	Pt mg/L	Mo mg/L	Pt content (wt%)[a]
Pt−Mo−200	MoS_{2-x}	240.14	368.8	10.7
Pt−(Mo−H)−200	Mo–H	440.49	2.55	7.7

[a] Pt content in the catalyst was calculated based on the Pt ion concentration in the remained impregnation solution after solid−liquid separation.

Table S3. Physical and chemical properties of Pt–MoS$_{2-x}$ catalysts

Catalysts	Pt content (wt%) [a]	Pt/S/Mo [b]	Pt (%)		Surface area (m^2/g)	Sulfur vacancy number (g^{-1})
			Pt^0	Pt^{2+}		
MoS$_{2-x}$	/	0:1.81:1	/	/	178.4	7.52×10^{16}
Mo–H	/	0:1.74:1	/	/	173.6	4.23×10^{17}
Pt–Mo	/	0.21:2.05:1	0	83.7	158.5	8.74×10^{16}
Pt–Mo–200	10.9	0.18:1.76:1	45.7	54.3	149.1	4.11×10^{17}
Pt−(Mo–H)	/	0.12:1.74:1	8.5	80.7	142.4	3.11×10^{17}
Pt−(Mo–H)−200	8.0	0.10:1.73:1	45.2	54.8	158.8	5.92×10^{17}

[a] Pt content was measured by ICP.

[b] S/Mo atom ratio on the catalyst surface was calculated based on the XPS data.
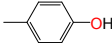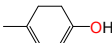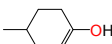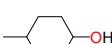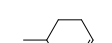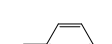
Table S4. Effect of Pt loading amount on the catalytic performance of Pt−MoS$_{2-x}$ in the HDO of

p−cresol[a]

Entry	Catalysts	Pt (wt%)	t (h)	Catalytic performance (%)				D. D. (%)
				Conversion	Cycloalkanes	Aromatics	Alcohols	
1	Mo−200[a]	0	8	3.9	20.1	45.6	None	3.5
2	Pt−Mo−X1	3.1	8	95.5	89.8	10.2	None	95.2
3	Pt−Mo−X2	6.8	5	95.9	91.4	9.6	None	95.5
4	Pt−Mo−X3	10.2	3	96.5	95.7	4.3	None	96.2
5	Pt−Mo−X4	10.9	2	95.5	94.7	5.3	None	95.1

[a] Reaction conditions: 2.4 g p−cresol, 0.1 g catalyst, 5 MPa hydrogen pressure, 140 °C reaction temperature.
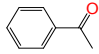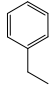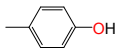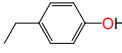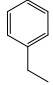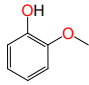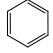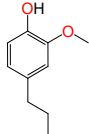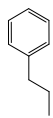
[a] Reaction temperature was 160 °C.

Table S5. The adsorption energies of p-cresol and intermediates on MoS_{2-x} and Pt/MoS_{2-x}[a]

Entry	Species	Adsorption energy (eV)	
		MoS_{2-x}	$Pt-MoS_{2-x}$
1	⟨OH⟩	−0.65	−2.09
2	⟨OH⟩	−0.68	−2.67
3	⟨OH⟩	−0.67	−2.33
4	⟨=O⟩	−0.46	−1.69
5	⟨OH⟩	−0.38	−1.16
6	⟨⟩	−0.64	−2.32
7	⟨⟩	−0.29	−1.10

[a] The adsorption energy of species is defined as: $E_{i\,[Adsorption]} = E_{i\,[total\ energy]} - E_{[catalyst]} - E_i$

Table S6. HDO of simulated lignin−derived bio−oil on Pt−Mo−200 [a]

Entry	Reactant	Weight (g)	Conversion (%)	Cycloalkanes selectivity (%)
1		0.6 g	100	>99
2		0.54 g	100	>99
3		0.62 g	100	>99
4		0.31 g	100	>99
5		0.41 g	100	100

[a] Reaction conditions: 0.1 g catalyst, 5 MPa hydrogen pressure, 160 ºC reaction temperature.

Table S7. Total carbon yield in the HDO of lignin–derived bio–oil on Pt−Mo−200
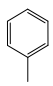
Entry	Carbon yield (%)
Carbon in monomers	46.9
Carbon in the products after volatilization	41.2
Total carbon	88.1

The calculation for total carbon yield

The elemental analysis showed that the carbon content in the lignin oil and products oil were 59.1% and 83.6%, respectively.

Part 1 Monomers

Equation:

The mass of the monomer was determined by GC-FID with n-tridecane as an internal standard.

The internal standard curve equation: Y=AX,

$$Y \text{ ——— } \frac{The\ peak\ area\ of\ monomer}{The\ peak\ area\ of\ n-tridecane};$$

X —— The concentration of monomer, mg/mL;

A —— Coefficient

The mass of the monomer =

$$\frac{(\frac{the\ peak\ area\ of\ monomer}{the\ peak\ area\ of\ n-tridecane})}{A} \times \text{the volume of the reaction mixture}$$

In the qualification process, the concentration of n-tridecane in the internal standard curve is the same as the concentration of n-tridecane in the reaction mixture.

For example, the reaction mixture in Figure S15 is the same sample in Table S6, the mass of cyclohexane (product **1** in Figure S15) was calculated as follows,

The internal standard curve equation of cyclohexane: $Y = 0.8498X$

The volume of the reaction mixture was 15 ml, the peak areas of cyclohexane and n-tridecane were 72.7 mv × min and 630 mv × min, respectively,

The mass of cyclohexane $= \dfrac{(\frac{72.7}{630})}{0.8498} \times 15 = 2.0$ mg

The carbon yield of the monomer (%)

$$= \frac{the\ mass\ of\ the\ monomer \times percent\ of\ carbon\ in\ the\ monomer}{the\ mass\ of\ lignin\ oil \times percent\ of\ carbon\ in\ oil} \times 100\%$$

For example:

Percent of carbon in cyclohexane (formula: C_6H_{12}) = 12*6/(12*6 + 12) = 0.8563

Percent of carbon in lignin oil is 0.591 according to elemental analysis,

The carbon yield of cyclohexane (%)

$$= \frac{the\ mass\ of\ cyclohexane \times percent\ of\ carbon\ in\ cyclohexane}{the\ mass\ of\ lignin\ oil \times percent\ of\ carbon\ in\ oil} \times 100\%$$

$$= \frac{2.0\ mg \times 0.8563}{100\ mg \times 0.591} = 2.8\%$$

Part 2 Products after volatilization

The mass of the products after volatilization (Products oil) is 29.1 mg.

The carbon yield of the products after volatilization (%)

$$= \frac{the\ mass\ of\ the\ liquid\ products\ after\ volatilization \times percent\ of\ carbon}{the\ mass\ of\ lignin\ oil \times percent\ of\ carbon} \times 100\%$$

$$= \frac{29.1\ mg \times 0.836}{100\ mg \times 0.591} = 41.2\%$$

Total carbon yield

Total carbon yield

= the carbon yield of monomers + the carbon yield of the products after volatilization

=46.9% + 41.2% = 88.1%

Table S8 The elemental analysis of lignin oil and upgraded lignin oil

Sample	C (wt%)	H (wt%)	O (wt%)	N (wt%)	S (wt)
Lignin oil	59.1	7.2	30.7	3.0	0
Upgraded lignin oil	83.6	11.3	3.5	1.6	0

The oxygen content in upgraded lignin oil was decreased from 30.7 wt% to 3.5 wt%. To eliminate the effect of the residual water, water was measured and its content was 15.8 ppm in the upgraded lignin oil, which contributed to 1.4 wt% oxygen content. Hence, the actual oxygen content in the upgraded lignin oil was only 2.1 wt%.